Nghiên cứu tối ưu quá trình gia tốc động cơ không đồng bộ ba pha

TÓM TẮT

Bài viết này trình bày nghiên cứu quá trình tăng/giảm tốc (gia tốc) của động cơ không đồng bộ ba pha trong quá trình khởi động và dừng nhằm nâng cao chất lượng hiệu quả truyền động cho động cơ. Dựa trên điều khiển tốc độ và mômen, tác giả xây dựng quỹ đạo tăng tốc S bậc cao nhằm khắc phục các hạn chế của gia tốc tuyến tính như hiệu suất thấp, rung lắc, giật và ảnh hưởng đến tuổi thọ hệ thống. Các kết quả mô phỏng cho thấy rằng việc sử dụng quỹ đạo S không chỉ giúp giảm độ giật mà còn hạn chế dao động momen, từ đó cải thiện rõ rệt độ êm ái và hiệu suất hệ truyền động. Ngoài ra, thuật toán xây dựng quỹ đạo S trong gia tốc đã được hiện thực hóa trên phần mềm và cấu hình trên nền tảng phần cứng FPGA. Kết quả thử nghiệm mô phỏng phần mềm, phần cứng cho thấy tín hiệu điều khiển tốc độ được tạo ra với độ phân giải và thời gian đáp ứng cao, phù hợp để tích hợp vào các hệ thống truyền động của động cơ không đồng bộ.

Từ khóa: Động cơ không đồng bộ, truyền động, quá trình gia tốc, quỹ đạo S, FPGA

Study on Optimal Acceleration Control of Three Phase Induction Motors

ABSTRACT

This paper presents a study on the acceleration and deceleration process of a three phase induction motor during start up and stop phases, aiming to enhance the dynamic performance of the drive system. Based on torque and speed control principles, the author proposes the application of a high order S-curve acceleration profile to overcome the limitations of linear acceleration, such as reduced efficiency, mechanical vibrations, jerks, and shortened system lifespan. Simulation results demonstrate that the S-curve profile not only reduces jerk but also minimizes torque oscillations, significantly improving the smoothness and overall performance of the drive system. Furthermore, the S-curve profile generation algorithm has been implemented in software and deployed on an FPGA hardware platform. Both software and hardware simulation results confirm that the generated speed control signals achieve high resolution and fast response, making the solution well suited for integration into induction motor drive systems.

Keywords*: Induction motor, drive system, acceleration process, S-curve profile, FPGA.*

1. INTRODUCTION

The acceleration and deceleration process of a three phase induction motor directly affects system efficiency, equipment durability, and the overall lifespan of the drive system. If the acceleration is too slow, it may overload the electrical system and delay motion execution; on the other hand, overly fast acceleration leads to large mechanical forces, vibrations, and early wear. Particularly in elevator applications, sudden changes in speed can cause discomfort, loss of balance, or even health concerns for elderly passengers and children.

Therefore, optimizing the acceleration process not only improves operational efficiency and system reliability but also enhances smoothness and extends mechanical durability in drive applications.

One of the key factors influencing operational quality is the acceleration profile applied during start and stop phases. Currently, linear acceleration profiles are commonly used in inverter based drives; however, they generate high jerk levels at phase transitions, leading to load oscillations, reduced mechanical component lifespan, and degraded user experience. In contrast, S-curve acceleration allows for much smoother motion, making it better suited for high precision systems such as CNC machines, elevators, and camera positioning systems.

The application of Field Oriented Control (FOC) aims to achieve rapid system stabilization and minimal tracking error, even under variations in motor parameters, load conditions, and external disturbances.[1],[2] However, the use of conventional linear acceleration profiles within FOC often results in high jerk, adversely affecting the mechanical load despite the fact that this method remains widely adopted in practice.

FOC and Direct Torque Control (DTC) are the two most common vector control strategies used in electric motor drive systems. FOC employs linear controllers and pulse-width modulation (PWM) techniques to regulate the fundamental voltage components applied to the stator.[3] In contrast, DTC is a nonlinear control approach that directly generates voltage vectors without the need for a modulation unit.

Studies such as [4] have presented comparative analyses between these two control strategies. The advantages and limitations of each method are analyzed specifically for two types of electric machines: the induction motor (IM) and the permanent magnet synchronous motor (PMSM). The comparisons are based on several evaluation criteria, including fundamental control

characteristics, dynamic performance, parameter sensitivity, and implementation complexity.

In paper [5], the author proposed a motor speed control method based on an artificial neural network incorporating an online learning algorithm, aimed at compensating for uncertain parameters and large load variations in the dynamic model of an AC motor. Simulation results conducted in MATLAB demonstrated the high control quality and effectiveness of the proposed method, clearly reflecting its strong adaptability when using an online-trained neural network.

Another study also introduced a solution based on a recurrent fuzzy neural network (RFNN) to address this limitation. Specifically, a traditional PID controller was combined with an RFNN-based supervisory controller to dynamically adjust the system's feedback response.[6] Simulation results showed that, under the same set of parameters, the system exhibited significant overshoot when using only the PID controller. However, when combined with the RFNN supervisory layer, the overshoot phenomenon was completely eliminated.

In studies [7],[8], a novel adaptive control scheme based on an improved Feedback Error Learning (FEL) method was proposed to address the Load Frequency Control problem. The FEL strategy incorporates both an intelligent controller and a conventional controller operating in the feedforward and feedback paths, respectively. In this scheme, the conventional feedback controller specifically a PID controller, plays a crucial role in ensuring global asymptotic stability of the system. Simultaneously, an intelligent feedforward controller (INFC) is employed to learn the inverse dynamics of the control system. Once the INFC successfully learns the system inverse, reference signal tracking can be achieved accurately during acceleration.

The aforementioned studies primarily aim to achieve fast control response, without fully addressing the issue that such rapid responses can lead to increased jerk, mechanical vibrations, and reduced lifespan of the drive system.

The problem of acceleration based on S-curve trajectories has been widely investigated, particularly in stepper and servo motors.[9],[10] In such systems, abrupt stopping, sudden starting, or rapid speed changes can cause the rotor to lose synchronization due to sudden changes in input pulses or mismatched pulse frequencies. This may lead to step loss, overshoot, and positional errors during motion. Additionally, strong impacts in the mechanical structure may shorten the system's operational life.

To mitigate these motion errors and improve motor stability, various control strategies have been proposed. Experimental results indicate that gradually reducing the speed of stepper motors significantly improves motion stability. However, if the speed is reduced too much, overall performance is compromised. Therefore, designing motor controllers that incorporate well-defined acceleration and deceleration phases can significantly enhance motion efficiency while ensuring smooth operation of the stepper motor.[11],[12]

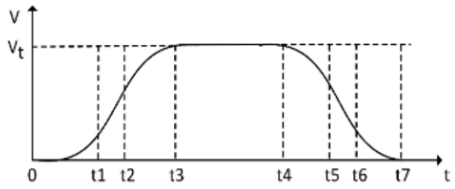

Figure 1. Seven phase S-curve acceleration profile. [13]

In addition to servo motors, [14] stepper motors have also been studied for acceleration control in camera motion applications.[15] To ensure accurate camera positioning and maintain visual continuity during motion, smooth speed control of the stepper motor is essential.

In elevator drive systems, induction motors must ensure high stopping accuracy while providing maximum comfort for passengers.[16] Moreover, elevators are characterized by frequent start-stop operations, requiring specialized braking systems and reliable speed feedback mechanisms.[17] The referenced study introduces various types of variable-speed drive systems and how they are applied in electric elevator systems.

Recently, some researchers have proposed jerk-reducing drive strategies for elevator applications.[18] However, these studies remain at a fundamental level and have not yet integrated with advanced control strategies for stabilizing both speed and torque.

Thus, previous studies have focused on two main directions:
The first direction investigates control methods for induction motors, aiming for speed tracking control that enables the motor speed to quickly respond to the reference speed, without yet addressing the impact of jerk on the load. The second direction explores the acceleration process using S-curve trajectories, with

consideration for jerk reduction, but primarily applied to stepper and servo motors in certain applications such as CNC machines, cameras, etc. FOC for controlling speed and torque, combined with high-order S-curve acceleration during startup, helps optimize operational efficiency, reduce power consumption, and extend lifespan and is the chosen solution in this paper.

2. IMPLEMENTATION CONTENT

2.1. Kinematic model of a three phase induction motor

The electromagnetic model of an induction motor is commonly represented in the dq reference frame (rotor flux-oriented), which simplifies torque and speed control when using an inverter. The fundamental equations of this model are as follows: [19]

$$\begin{cases} v_d = R_s i_d + \dfrac{d\psi_d}{dt} - \omega_e \psi_q \\ v_q = R_s i_q + \dfrac{d\psi_q}{dt} - \omega_e \psi_d \\ \psi_d = L_d i_d + L_m i_{dr} \\ \psi_q = L_q i_q + L_m i_{qr} \end{cases} \quad (1)$$

Where:

i_d, i_q : Stator current in the dq axis (A)

v_d, v_q : Stator voltages in the dq axis (V)

ψ_d, ψ_q: dq axis flux linkages (Wb)

ω_e : Electrical angular speed (rad/s)

R_s: Stator resistance (Ω)

L_d: Inductance (H)

The electromagnetic torque is calculated as follows:

$$M_e = \frac{3}{2} p.L_m.(i_{qs} i_{dr} - i_{ds} i_{qr}) \quad (2)$$

The inverter is a device that controls the voltage and frequency supplied to an induction motor, enabling precise adjustment of the motor's rotational speed. In motor drive systems, accurate speed control is essential to prevent vibrations during start and stop operations and to maintain stability under varying load conditions. In this study, the authors propose a vector control approach specifically FOC [1] combined with the design of an S-curve acceleration profile to enhance motion smoothness and drive performance (**Figure 2**).

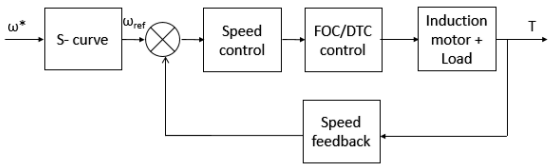

Figure 2. Speed control model with integrated S-curve acceleration profile

2.2. Xây dựng thuật toán tăng/giảm tốc

Phương trình mô tả độ giật (3), yếu tố ảnh hưởng đến chất lượng gia tốc cho động cơ không đồng bộ.

$$j(t) = \frac{da(t)}{dt} \quad (3)$$

The standard form of this trajectory divides the motion into seven phases, ensuring a continuous change in acceleration (**Figure 1**): Increasing jerk up to j_{max}, increasing acceleration up to a_{max}; Reducing jerk back to zero → maintaining constant velocity; Applying negative jerk down to − j_{max}; Reducing acceleration back to zero → preparing to stop.

An S-curve velocity trajectory is twice differentiable, meaning that both the velocity and acceleration profiles are continuous functions. Let v(t) represent an S-curve velocity trajectory defined over the interval [0, T]. Then, for every t∈[0,T], we have:

$$\begin{aligned} v'(t) &= v'(0) + \int_0^t v''(w)dw \\ v(t) &= v(0) + \int_0^t v'(w)dw \end{aligned} \quad (4)$$

The velocity profile v(t) must also satisfy certain boundary conditions. Assuming $v(0)=v_s$ and $v(T) = v_e$, for computational convenience, the profile v(t) can be divided into three segments:

a) Acceleration over the time interval [0, t_a], during which the velocity increases from v_s to v_m, where t_a is the acceleration time.
b) Deceleration over the time interval [T−t_d, T], during which the velocity decreases from v_m to v_e, where t_d is the deceleration time.
c) Constant velocity over the time interval (t_a, T−t_d), during which the velocity maintains a fixed value v_m.

Given an initial point and a final point with physical constraints and boundary conditions as described, we set $v_m''=v_{max}''$ in our proposed S-curve velocity profile to allow acceleration or deceleration to change as rapidly as possible

when needed. We then seek an optimal value for v_m under the constraint of total travel distance and subject to the conditions $v_s < v_m \le v_{max}$ and $v_e < v_m \le v_{max}$, which results in solutions for the acceleration segment, deceleration segment, and constant velocity segment.

The increasing boundary of the S-shaped velocity curve is symmetric about its midpoint $\left(\frac{t_a}{2}, \frac{v_m + v_s}{2}\right)$. Accordingly, the acceleration phase over the time interval [0, t_a] can be subdivided into three subregions corresponding to the previously described stages.

$$v(0) = v_s \qquad v(t_a) = v_m \tag{5}$$

$$v'(0) = 0 \qquad v'(t_a) = 0 \qquad v'(t) = v'_m, t_j \le t \le t_a - t_j \tag{6}$$

$$v''(t) = \begin{cases} v''_m, & 0 \prec t \prec t_j \\ 0, & t_j \le t \le t_a - t_j \\ -v''_m, & t_a - t_j \prec t \prec t_a \end{cases} \tag{7}$$

Where v_m, v'_m và v''_m are constants satisfying the conditions: $v_s \prec v_m \prec v_{\max}, v'_m \le v'_{\max}$ and $v''_m = v''_{max}$.

Assuming an initial value v_m is given, along with the corresponding solutions for the acceleration (rising) and deceleration (falling) segments, there are two possible cases concerning the displacement constraint:

Case 1:

$$\int_0^{t_a} v(t)dt + \int_{T-t_d}^{T} v(t)dt \le l \tag{8}$$

We have:

$$v_m\left(T - t_a - t_d\right) = l - \frac{1}{2}\left[\left(v_m + v_s\right)t_a + \left(v_m + v_e\right)t_d\right] \tag{9}$$

$$T = t_a + t_d + \frac{1}{v_m}\left\{l - \frac{1}{2}\left[\left(v_m + v_s\right)t_a + \left(v_m + v_e\right)t_d\right]\right\} \tag{10}$$

Case 2:

$$\int_0^{t_a} v(t)dt + \int_{T-t_d}^{T} v(t)dt \succ l \tag{11}$$

We must reduce the value of vmv_mvm and recalculate the acceleration and deceleration segments to ensure that the displacement constraint is satisfied. The S-curve velocity profile can be solved and optimized using the following binary search method.

Given the maximum velocity v_{max}, maximum acceleration a_{max}, and maximum jerk j_{max}, with boundary conditions $v(0) = v_s$, $v(T) = v_e, t_j, t_a, t_{-j}$ and t_d the profile components become functions of v_m, and are expressed as follows:

$$t_j = \begin{cases} \sqrt{\frac{v_m - v_s}{v''_{max}}}, & \sqrt{v''_{max}\left(v_m - v_s\right)} \le v'_{max} \\ \frac{v'_{max}}{v''_{max}}, & \sqrt{v''_{max}\left(v_m - v_s\right)} \succ v'_{max} \end{cases} \tag{12}$$

$$t_a = \begin{cases} 2t_j, & \sqrt{v''_{max}\left(v_m - v_s\right)} \le v'_{max} \\ \frac{v_m - v_s}{v'_{max}} + t_j & \sqrt{v''_{max}\left(v_m - v_s\right)} \succ v'_{max} \end{cases} \tag{13}$$

$$t_{-j} = \begin{cases} \sqrt{\frac{v_m - v_e}{v''_{max}}}, & \sqrt{v''_{max}\left(v_m - v_e\right)} \le v'_{max} \\ \frac{v'_{max}}{v''_{max}} & \sqrt{v''_{max}\left(v_m - v_e\right)} \succ v'_{max} \end{cases} \tag{14}$$

$$t_d = \begin{cases} 2t_{-j}, & \sqrt{v''_{max}\left(v_m - v_e\right)} \le v'_{max} \\ \frac{v_m - v_e}{v'_{max}} + t_{-j}, & \sqrt{v''_{max}\left(v_m - v_e\right)} \succ v'_{max} \end{cases} \tag{15}$$

The algorithm is constructed as follows:[14]

The algorithm illustrated in **Figure 3** has been applied to design S-curve profiles of third, fourth, and fifth order. Equidistant sampling points are generated in the form of numerical arrays by the trajectory planning program. These profiles are then fed into the controller, which commands the induction motor to follow the corresponding S-curve motion. The higher the order of the curve, the smoother the resulting motion becomes.

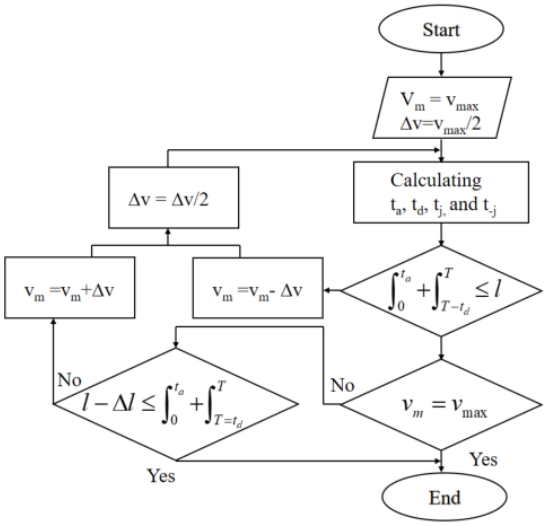

Figure 3. Flowchart of the S-Curve Trajectory Calculation Algorithm

2.3. Integration of S-curve profile with speed control

The S-curve profile generates smooth time-varying references for velocity, position, and torque. Control strategies such as FOC or DTC are responsible for accurately executing the required torque or velocity commands on the motor. Once the FOC controller is in place, it is necessary to generate speed or current (torque) reference signals that precisely follow the S-curve acceleration profile to control the motor accordingly.

The velocity profile $\omega_{ref}(t)$ is pre-generated as a time-based function. It is then compared with the actual motor speed $\omega_{act}(t)$, and a speed PI controller is used to regulate the current specifically, the torque producing current component i_q^*

$$\omega_{ref}(t) = a_0 + a_1 t + a_2 t^2 + a_3 t^3 + a_4 t^4 + a_5 t^5 \quad (16)$$

The coefficients a_i are calculated from the boundary conditions.

$\omega(0) = 0$, $\omega(T) = \omega_{max}$,

$\omega'(0) = \omega'(T) = 0$, $\omega''(0) = \omega''(T) = 0$

$$i_q^*(t) = PI\left[\omega_{ref}(t) - \omega_{act}(t)\right] \quad (17)$$

The FOC controller is responsible for converting input signals $i_q^*(t)$ into generated torque.

Direct generation of the reference torque $T_{ref}(t)$: The required acceleration is calculated $a(t) = \dot{\omega}_{ref}(t)$ from the S-curve trajectory, and then the necessary torque is determined accordingly.

$$T_{ref}(t) = J.a(t) \quad (18)$$

$$e(t) = \omega_{ref}(t) - \omega_{act}(t) \quad (19)$$

$$T_{PI}(t) = K_p e(t) + K_i \int e(t)dt \quad (20)$$

$$T_{total}(t) = T_{PI}(t) + T_{ref}(t) \quad (21)$$

$$i_q^*(t) = \frac{2}{3}\frac{T_{total}(t)}{p.\Psi_r} \quad (22)$$

Where:

p: Number of pole pairs

ψ_r : Rotor flux

The actual torque T_{act} (or the torque-producing current component i_q) is continuously compared with the reference torque $T_{ref}(t)$, and i_q is adjusted accordingly to ensure accurate torque tracking. The S-curve trajectory generator provides a time-based reference for either speed or torque. This reference is then used by the motor control system typically based on FOC or DTC to ensure the motor follows the desired S-curve profile with high precision.

3. SIMULATION RESULTS AND DISCUSSION

3.1. Tham số mô phỏng

Consider a specific case in which a three-phase squirrel-cage induction motor is used for elevator applications and driven through an inverter–motor drive system. Suppose we intend to implement the control strategy using a microcontroller integrated with the inverter.

Table 1. Simulation parameter table

Parameter	Value
Rated voltage	380 V
Rated frequency	50 Hz
Rated power	3.7 kW
Rated current	7.6 A
Number of poles	4 poles
Rated speed	1445 rpm
Total moment of inertia J	0.045 kg·m²
Stator resistance R_1	0.80 Ω
Rotor resistance (referred) R2′	0.85 Ω
Stator inductance L_1	0.0055 H
Rotor inductance L_2	0.0055 H
Magnetizing inductance L_m	0.140 H

3.2. Linear acceleration

The linear acceleration process is performed using the motor parameters provided above.

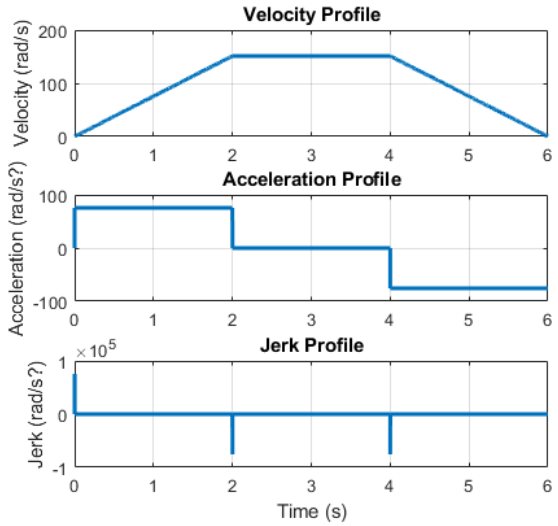

Figure 4. Linear acceleration simulation results

The simulation results of the linear acceleration and deceleration process for a 3.7 kW induction motor show that: The motor velocity increases linearly from 0 to its rated speed (1445 rpm) over a 2-second period, remains constant for another 2 seconds, and then decreases linearly back to zero in the final 2 seconds.

During the acceleration phase, the angular acceleration (a) remains constant and positive; it becomes zero during the constant-speed phase, and remains constant and negative during deceleration.

The jerk is approximately zero throughout the uniform acceleration and deceleration phases, except at the phase transitions → specifically at the end of acceleration (transition to constant speed) and the end of constant speed (transition to deceleration) → where sudden changes in acceleration produce large spikes in jerk.

The most significant jerk spikes are observed at the following transition points:

At time t = t_{acc} = 2 seconds: the acceleration phase ends and transitions into the constant-speed phase.

At time t = t_{acc} + T_{hold} = 4 seconds: the constant-speed phase ends and transitions into the deceleration phase.

At these two critical points, the acceleration abruptly shifts from a positive value during acceleration to zero at the start of the constant-speed phase, and from zero to a negative value at the start of deceleration. As a result, jerk spikes appear in the plots with extremely high magnitudes, resembling ideal impulse signals with almost instantaneous transitions.

This behavior indicates that acceleration changes instantaneously, with no transitional smoothing phase. As a consequence, both the motor and mechanical load are subjected to significant impulsive forces at the phase transitions.

These high jerk values cause mechanical shock on the motor shaft, drivetrain, and gear mechanisms, increasing the risk of premature failure. The sharp forces also introduce vibrational stresses, which reduce the service life of bearings, gears, and elevator cables. Furthermore, such impulsive dynamics may excite the mechanical system's resonant modes, resulting in unwanted vibrations. From a control perspective, the sudden demand for current and torque adjustment may lead to overshoot, thermal stress in the motor, and even overloading of the inverter system.

3.3. Higher-order acceleration

The velocity trajectory takes the form (16). Boundary conditions: v(0)=0, v(T)=v_{max} (initial, final velocity), a(0)=0, a(T)=0 (initial, final acceleration 0), j(0)=0, j(T)=0 (initial, final jerk 0).

The simulation results **(Figure 5)** of the acceleration constant speed deceleration process of a 3.7 kW motor following a 5th-order S-curve trajectory demonstrate that the velocity increases and decreases smoothly and continuously over time.

The acceleration no longer remains constant as in a linear profile, but instead gradually increases to a peak and then naturally decreases back to zero.

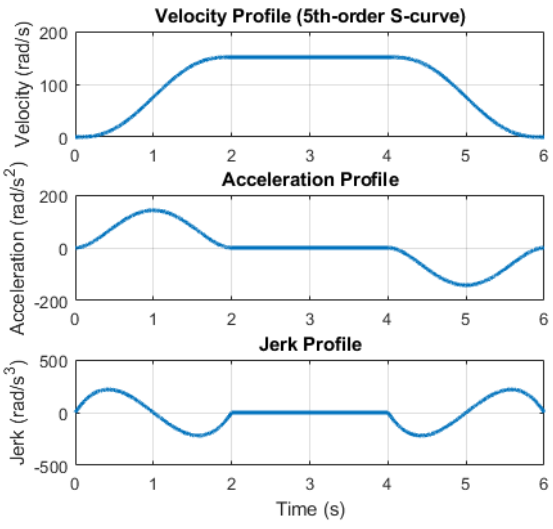

Figure 5. S-curve acceleration for the motor

Jerk does not exhibit sharp spikes as seen in linear acceleration profiles; instead, it varies smoothly with mild oscillations during phase transitions, ensuring higher-order continuity of the trajectory.

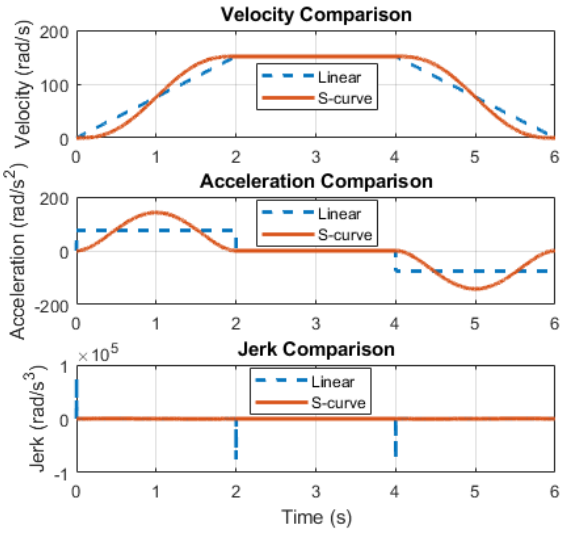

Figure 6. Comparison between linear acceleration and S-Curve acceleration

The simulation results **(Figure 6)** of the acceleration, constant speed, and deceleration phases of a 3.7 kW motor using two control strategies linear acceleration and 5th-order S-curve acceleration highlight significant differences in velocity, acceleration, and jerk profiles.

Both methods achieve the target speed (1445 RPM) within the same total duration. However, the velocity, acceleration, and jerk trajectories differ markedly in terms of continuity and smoothness.

Moment 1: End of acceleration phase ($t = t_{acc}$) In the case of linear acceleration/deceleration, the acceleration drops abruptly from a positive value to zero, resulting in a large jerk spike at the phase transition. This can cause mechanical shocks to the system and sudden inrush currents in the motor. In contrast, the 5th-order S-curve trajectory allows the acceleration to gradually decrease to zero before the end of the acceleration phase. Jerk varies smoothly without large spikes, leading to a gentle transition with no vibration or shock.

Moment 2: End of constant-speed phase, beginning of deceleration ($t = t_{acc} + t_{hold}$) For the linear profile, the acceleration changes abruptly from zero to a negative value, producing another large negative jerk spike. This sudden change may impose unexpected forces on mechanical components, increasing the risk of material fatigue or failure. With the S-curve profile, acceleration decreases smoothly from zero to its negative peak value. Jerk remains continuous, ensuring a soft deceleration phase and improving system durability.

Using linear acceleration, the mechanical system is subjected to abrupt stress at each phase transition due to high jerk, leading to material fatigue and reduced equipment lifespan. In contrast, the 5th-order S-curve ensures continuous changes in acceleration and jerk, distributing forces more evenly throughout the motion. This reduces mechanical shock, extends the lifespan of the motor, transmission components, and mechanical structure, and significantly enhances system smoothness and operational stability.

3.4. Integrated speed control with S-curve-based acceleration profile

S-curve velocity profile: ω(t) (rad/s); compute the angular acceleration a(t) and jerk j(t); calculate the reference torque T(t) based on the moment of inertia J:

The simulation results (**Figure 7**) demonstrate that the combination of S-curve acceleration trajectory planning and torque control using a PI controller with feedforward compensation achieves highly effective speed regulation. The actual motor speed closely follows the reference trajectory over time, with minimal deviation virtually eliminated even at phase transitions between acceleration, constant speed, and deceleration.

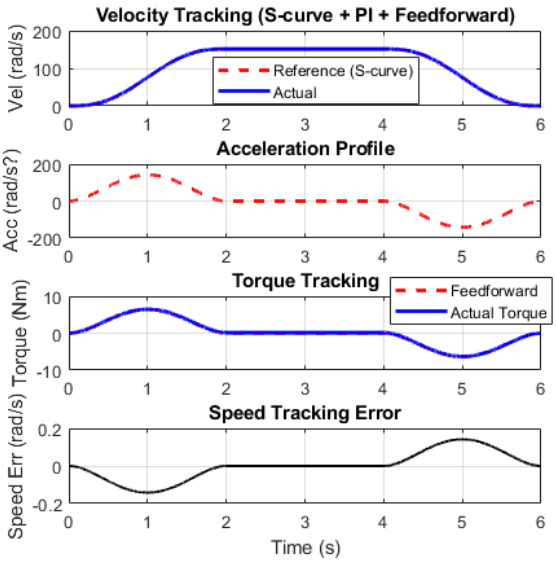

Figure 7. Torque control combined with S-curve acceleration

The motor torque is adjusted smoothly and continuously thanks to the feedforward torque component, which compensates based on the trajectory acceleration. This allows the motor to respond quickly to required velocity changes without relying entirely on PI feedback. As a result, the system achieves not only high tracking accuracy but also reduces the control burden on the feedback loop, minimizing overshoot and oscillation.

Compared to the model using a standalone PI controller, the addition of feedforward clearly yields smoother, more precise operation and significantly shortens the transient response time. This control strategy is well-suited for high-performance motion systems requiring precision and smoothness, such as premium elevators, industrial robots, or autonomous guided vehicles (AGVs).

3.5. Simulation of FPGA hardware implementation

The `step_out` signal generates pulses with a frequency that varies according to this profile, specifically: the maximum speed is 1445 RPM (approximately 151.3 rad/s), acceleration time is 2 seconds, the peak acceleration is around 200 rad/s², and the peak jerk is approximately 500 rad/s³.

Parameter	value
`CLK_PERIOD`	20 ns
`jerk_val`	1000
`accel_ticks`	5000
`start`	1 sau 200 ns
`sim_time`	10 ms

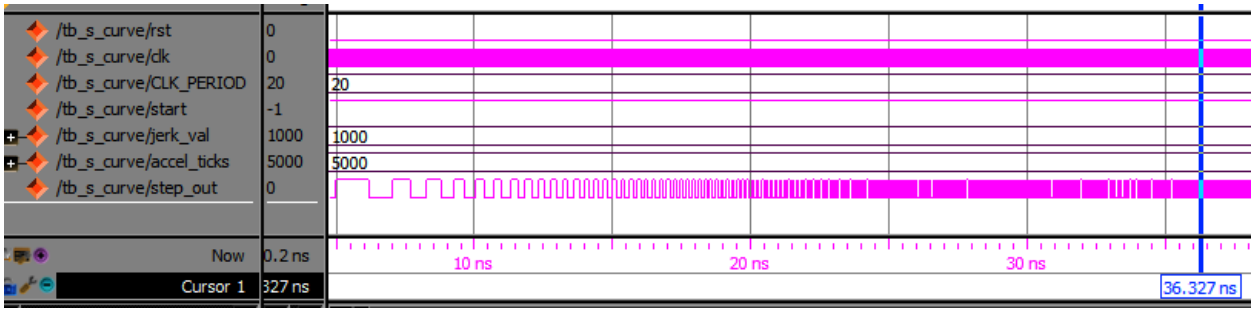

Figure 8. S-curve trajectory acceleration process on FPGA output pin

The simulation results (**Figure 8**) show that the `step_out` signal appears with gradually increasing frequency, reflecting a smooth acceleration process characteristic of an S-curve trajectory.

`jerk_val` *(unit: Δacc per clock cycle)*: Controls the rate of acceleration change. A higher value results in faster velocity increase.

`accel_ticks` *(number of clock cycles)*: Defines the total acceleration time. The larger this value, the slower and smoother the acceleration phase becomes.

`step_out`: Output pulse signal with frequency proportional to motor velocity. Observation shows that the pulses become increasingly dense over time consistent with the expected behavior of S-curve motion.

The simulation confirms that the system operates stably and without glitches, making it suitable for motor control applications requiring high precision and smoothness.

To evaluate the combined effect of S-curve acceleration/deceleration with speed and torque control during the initial 2-second period, the authors performed a scaled simulation in ModelSim using a 2 ms acceleration phase, followed by 2 ms of constant speed, and 2 ms of deceleration. This allows for easier verification and visualization within the simulation environment.

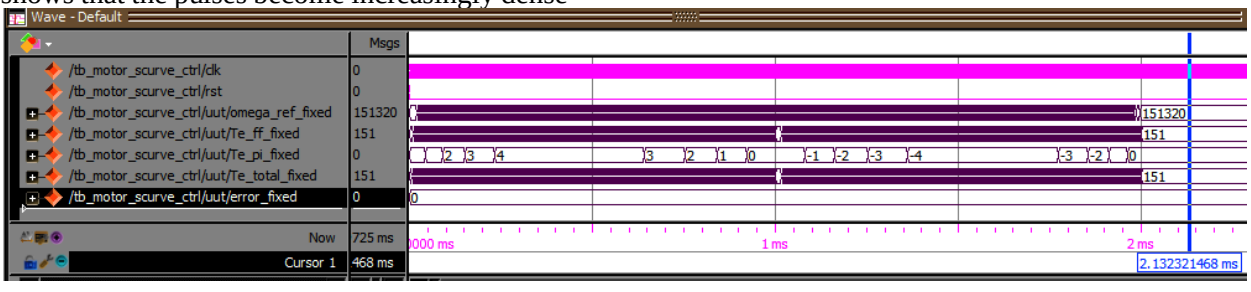

Figure 9. S-curve-based acceleration integrated with speed control

The simulation results (**Figure 9**) confirm the effectiveness of integrating a 5th-order S-curve motion profile with a combined PI and feedforward torque control strategy. The system achieves smooth velocity transitions, minimal tracking error, and continuous torque responses without overshoot or delay. The use of fixed-point quantization for velocity, acceleration, and torque signals makes the control scheme well-suited for FPGA implementation, enabling real-time processing and hardware efficiency.

The entire acceleration–deceleration process over a 4-second interval was accurately simulated on ModelSim and verified to be stable, responsive, and glitch-free. This validated model is ready for deployment in high-precision motion control applications, such as elevator drives, industrial automation, and autonomous vehicle motors using FPGA platforms.

4. CONCLUSION

This paper has presented an effective approach for implementing smooth and precise motion control by integrating a 5th-order S-curve trajectory with PI-based torque control enhanced by feedforward compensation. Simulation results confirm that the proposed method ensures smooth velocity transitions, continuous acceleration and jerk profiles, and stable torque responses, significantly improving motion quality and system stability.

The control strategy was successfully modeled and verified in ModelSim, where key motion parameters such as speed, acceleration, and torque were quantized using fixed-point representation. This design choice makes the solution highly suitable for real-time implementation on FPGA platforms. The system demonstrated glitch-free behavior, consistent pulse generation (`step_out`), and accurate speed tracking within a compact simulation window, confirming the feasibility of hardware deployment.

The main contributions of this work are:

Development of a 5th-order S-curve motion generator suitable for digital hardware implementation;

Integration of PI and feedforward speed control for improved tracking performance and response smoothness;

Verification of real-time behavior using a hardware-oriented simulation on ModelSim for optimized FPGA resource utilization;

Demonstration of applicability to high-precision motor drive systems such as elevators, industrial robots, and autonomous guided vehicles (AGVs).

Overall, the proposed model provides a practical and scalable foundation for implementing smooth acceleration and torque control in embedded motion systems using FPGA technology

REFERENCES

1. H. G. Herzog, M. A. W. Begh, “Comparison of Field Oriented Controland Direct Torque Control,” *TechRxiv - IEEE*, **2024,** no 12, pp. 1–16.
2. L. T. T. Phuong, L. T. T. Huyen, and P. T. H. Anh, “Application of rotor flux-oriented vector control for induction motors,” *Journal of Science and Technology*, **2017**, vol. 172, no. 1, pp. 115–119.
3. T. V. Thong and D. V. Can, “A proposal of multi-channel noise-reduction ADRC position control on FPGA for servo drive systems,” *Quy Nhon University Journal of Science*, **2018,** vol. 12, no. 3, pp. 91–102.
4. D. V. Can, “Current controller design based on FPGA,” *Quy Nhon University Journal of Science*, **2020**, vol. 15, no. 1, pp. 71–78.
5. K. Sabahi, M. Teshnehlab, and M. A. Shoorhedeli, “Recurrent fuzzy neural network by using feedback error learning approaches for LFC in interconnected power system,” *Energy Conversion and Management*, **2009,** vol. 50, no. 4. pp. 938–946.
6. N. C. Ngon. D. H. D. Khoa, S. H. Thanh, “Intelligent control of induction motor using recurrent fuzzy neural networks,” *TNU Journal of Science and Technology*, **2022**, vol. 227, no. 08, pp. 46–55.
7. M. A. F. Allam, Z. Nossair, H. Gomma, I. Ibrahim, “Evaluation of using a recurrent neural network (rnn) and a fuzzy logic controller (flc) in closed loop system to regulate blood glucose for type-1 diabetic patients,” *I.J. Intelligent Systems and Applications*, **2012**, vol. 10, pp. 58–71.
8. D. V. Can, “Design and development of a controller for servo drive systems,” *Quy Nhon University Journal of Science*, **2016**, vol. 2, no. X.
9. B. Kumar, P. Wang, and A. S. Hossain, “Design of Motion Profile of Stepper Motor for Elevator Using Arduino Uno,” *North*

American Academic Research Journal, **2020**, vol. 3, no. 04, pp. 683–695.
10. A. Drumea, C. I. Marghescu, M. P. Ă, G. Jitianu, and A. Vlad, "S-curve motion control implementation using 32-bit microcontroller," in *Proceedings of 2022 International Conference on Hydraulics and Pneumatics - HERVEX November 9-10,* **2022,** *Băile Govora, Romania*, pp. 160–165.
11. Z. Zhang and Y. Yu, "S-type speed control curve based on the number of pulses," *Journal of Physics: Conference*, **2022,** Vol 2196, pp 1-10.
12. V. Kombarov, V. Sorokin, O. Fojtů, Y. Aksonov, and Y. Kryzhyvets, "S-curve algorithm of acceleration/ deceleration with smoothly-limited jerk in high-speed equipment control tasks," *MM Science Journal*, **2019**, vol. 102, no. November, pp. 3264–3270.
13. C. Li and F. Chen, "Application of S-curve Acceleration and Deceleration in Winding of Bond-Wire," *International Journal of Trend in Research and Development*, **2021**, vol. 8, no. 4, pp. 158–161.
14. X. Li, "Optimizing S-curve Velocity for Motion Control," *Far East Journal of Applied Mathematics*, **2010**, no, 24, pp. 1–12.
15. X. Wei, "Acceleration and deceleration control design of step motor based on TMS320F240," *Procedia Eng. Elsevier*, vol. 15, pp. 501–504, 2011.
16. V. I. Vlachou, D. E. Efstathiou, and T. S. Karakatsanis, "Design, Analysis and Application of Control Techniques for Driving a Permanent Magnet Synchronous Motor in an Elevator System," *MPDI Machines*, **2024**, vol. 12, no 8.
17. R. Akçelik and M. Besley, "Acceleration and deceleration models," *Conference of Australian Institutes of Transport Research*, January **2001**, pp. 107–156.
18. M. Osama and O. A. Azim, "Implementation and performance analysis of an elevator electric motor drive system," *12th International Middle East Power System Conference*, **2008**, pp. 114–118.
19. D. V. Can and T. X. Khoa**,** "Research and design of a position controller based on FPGA," *The 7th International Conference and Exhibition on Control and Automation - VCCA*, **2024**, pp 109-115.